Induced Conformational Change on Ferrocenyl-Terminated Alkyls and its Application as a Transducer for a Label-Free Immunosensing of Alzheimer's Disease Biomarker.

Abdelmoneim Mars,[a] Wicem Argoubi,[a] Sami Ben Aoun[b]* and Noureddine Raouafi [a]*
University of Tunis El-Manar, Chemistry Department, Laboratory of Analytical Chemistry and Electrochemistry (LR99ES15), Campus Universitaire de Tunis El-Manar 2092, Tunis, Tunisia. *Corresponding author: Noureddine Raouafi (n.raouafi@fst.rnu.tn), Tel.: +21671872600 (Ext. 273); Fax: +21671883424
Department of Chemistry, Faculty of Science, Taibah University, PO. Box 30002 Al–Madinah Al–Munawarah, Saudi Arabia. *Corresponding author: Sami Ben Aoun (sbenaoun@taibahu.edu.sa), Tel.: +966590900727; Fax: +966148618888 (Ext. 4326)

Abstract

Alzheimer's disease is the second most common neurogenerative illness affecting elderly people. Early diagnostic could help improving the patients' life quality. The classical sandwich ELISA-based methods are usually costly and time consuming. In this study, we report the design of a label-free immunosensing platform for the sensitive detection of ApoE protein as a biomarker of Alzheimer's disease. The immunorecognition event induces conformational changes in ferrocenylalkyl tethered to the superficial gold nanoparticles in the vicinity of the antibody. The heavy antigen/antibody complex enhances the electron-transfer (ET) rate constants by bending the ferrocenylalkyl chain bringing the ferrocene closer to the gold surface. Determination of the ET rate constants and the analytical performance studies for a series of devices using ferrocenylakyl with different chain lengths support the proposed mechanism. The best performances and the highest rate constants are observed with sensors having the most flexible chains. The devices are endowed with a large dynamic range (i.e. 0.13 to >1880 ng.mL^{-1}) and excellent selectivity and specificity.

Keywords

ApoE Immunosensing; Conformational Changes; Electron-Transfer Rate Constant; Ferrocene; Gold nanoparticles.

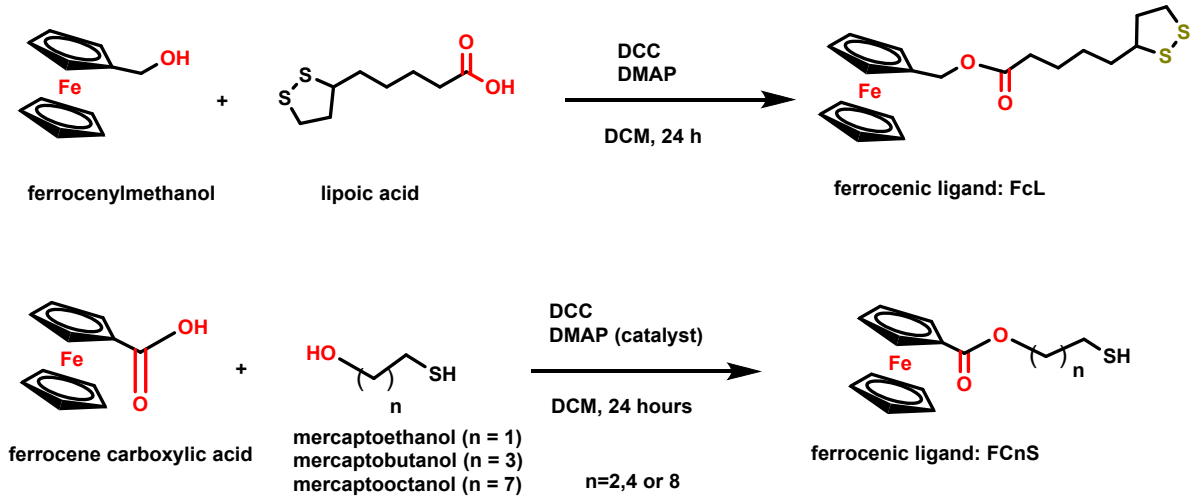

Fig. S1. Schematic route for synthesis of ferrocenylalkyl derivatives.

NMR data

Compound FC_8S

^1H NMR δ_H (300.13 MHz, $CDCl_3$, TMS): 1.38-1.76 (14H, m, $S(CH_2)_7$), 4.08 (2H, m, OCH_2), 4.21 (5H, s, Fc, CH), 4.32 (2H, s, Fc, CH), 4.81 (2H, s, Fc, CH), ^{13}C NMR δ_C (75.1 MHz, $CDCl_3$, TMS): 26.6 (s, $S(CH_2)_5CH_2$), 28.7 (s, $S(CH_2)_2CH_2$), 29.1 (s, $S(CH_2)_3CH_2$, $S(CH_2)_4)CH_2$), 29.4 (s, $S(CH_2)_6CH_2$), 32.8 (s, SCH_2), 33.8 (s, SCH_2CH_2) 64.4 (s, OCH_2), 70.1 (s, Fc, CH), 71.2 (s, Fc, CH), 71.6 (s, Fc, C_q), 172 (s, CO_2).

Compound FC_4S

^1H NMR δ_H (300.13 MHz, $CDCl_3$, TMS): 1.41-1.95 (5H, m, SH, $HS\text{-}CH_2\text{-}(CH_2)_2\text{-}CH_2O$), 2,81-2,91 (2H, m, $HS\text{-}CH_2$), 4.13 (2H, m, OCH_2), 4.27 (5H, s, Fc, CH), 4.33 (2H, s, Fc, CH), 4.84 (2H, s, Fc, CH), ^{13}C NMR δ_C (75.1 MHz, $CDCl_3$, TMS): 26.4 (s, $S(CH_2)_5CH_2$), 28.3 (s, $S(CH_2)_2CH_2$), 29.3 (s, $S(CH_2)_3CH_2$, $S(CH_2)_4)CH_2$), 29.6 (s, $S(CH_2)_6CH_2$), 32.4 (s, SCH_2), 34.2 (s, SCH_2CH_2) 64.9 (s, OCH_2), 70.1 (s, Fc, CH), 71.2 (s, Fc, CH), 71.8 (s, Fc, C_q), 172 (s, CO_2).

Compound FC_2S

^1H NMR δ_H (300.13 MHz, $CDCl_3$, TMS): 2.78-2.96 (2H, m, $HS\text{-}CH_2$), 4.15 (2H, m, OCH_2), 4.27 (5H, s, Fc, CH), 4.34 (2H, s, Fc, CH), 4.82 (2H, s, Fc, CH), ^{13}C NMR δ_C (75.1 MHz, $CDCl_3$, TMS): 26.8 (s, $S(CH_2)_5CH_2$), 28.9 (s, $S(CH_2)_2CH_2$), 29.3 (s, $S(CH_2)_3CH_2$, $S(CH_2)_4)CH_2$), 29.4 (s,

$S(CH_2)_6CH_2$), 32.7 (s, SCH_2), 34,1 (s, SCH_2CH_2) 64.7 (s, OCH_2), 70.1 (s, Fc, CH), 71.3 (s, Fc, CH), 71.7 (s, Fc, C_q), 172 (s, CO_2).

Compound FcL

^{1}H NMR δ_H (300.13 MHz, $CDCl_3$, TMS): 1.15-1.31 (4H, m, $CO(CH_2)_2CH_2$, $CO(CH_2)_3CH_2$), 1.55 (2H, m, $COCH_2CH_2$), 1.85 (2H, m, $SSCH_2CH_2$), 2.1-2.34 (2H, m, $COCH_2$), 3.13 (2H, m, $SSCH_2$), 3.54 (1H, m, SSCH), 4.11 (s, 5H, CHCp), 4.21 (2H, s, C_βH-Cp), 4.29 (2H, s, C_αH-Cp), 4.23 (t, 2H, $FcCH_2CO_2$). ^{13}C NMR δ_C (75.1 MHz, $CDCl_3$, TMS): 27.0 ($COCH_2CH_2$); 29.2 ($CO(CH_2)_2CH_2$, $CO(CH_2)_3CH_2$); 34.7 ($SSCHCH_2$); 39.8 ($SSCH_2$); 40.3 ($SSCH_2CH_2$); 56.6 (SSCH); 64.1 ($FcCH_2CO_2$); 70.1-71.2 (C, Cp); 77.5 (Cp, Cq); 174.0 (CO_2).

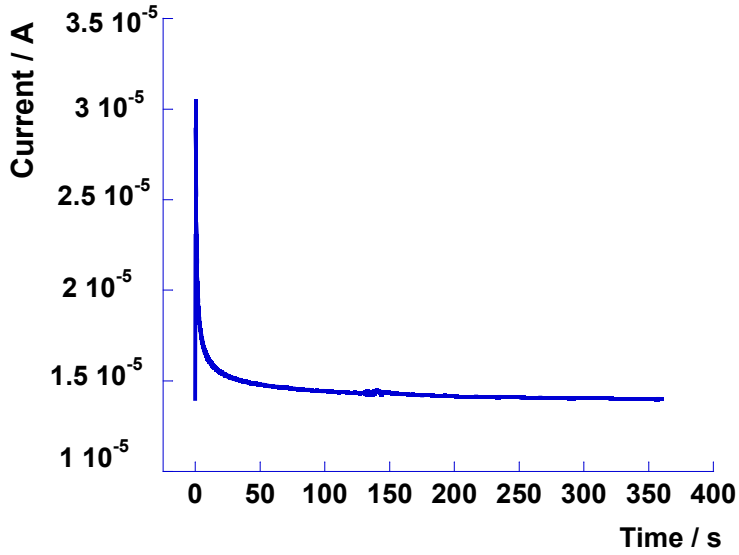

Fig. S2. Chronoamperogram of electrochemically assisted adsorption of ferrocene derivative on gold nanoparticles.

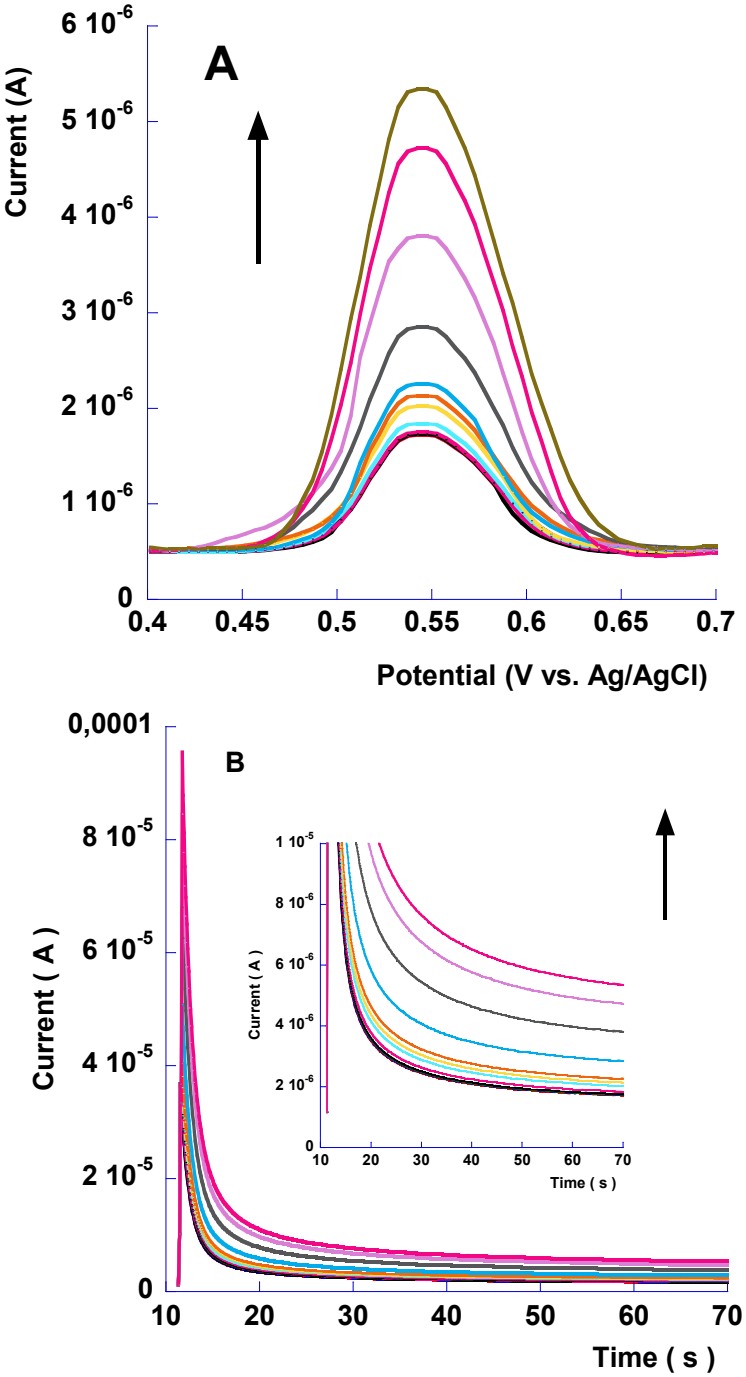

Fig. S3. Variation in the DPV current in the Ferrocene FC_2S/α-ApoE based immunosensor evidencing ApoE/α-ApoE recognition after incubation in ApoE solutions with gradually increasing concentrations (A) and variation in chronoamperometry current of Ferrocene FC_2S immunosensor after incubation in progressive ApoE concentrations (B).

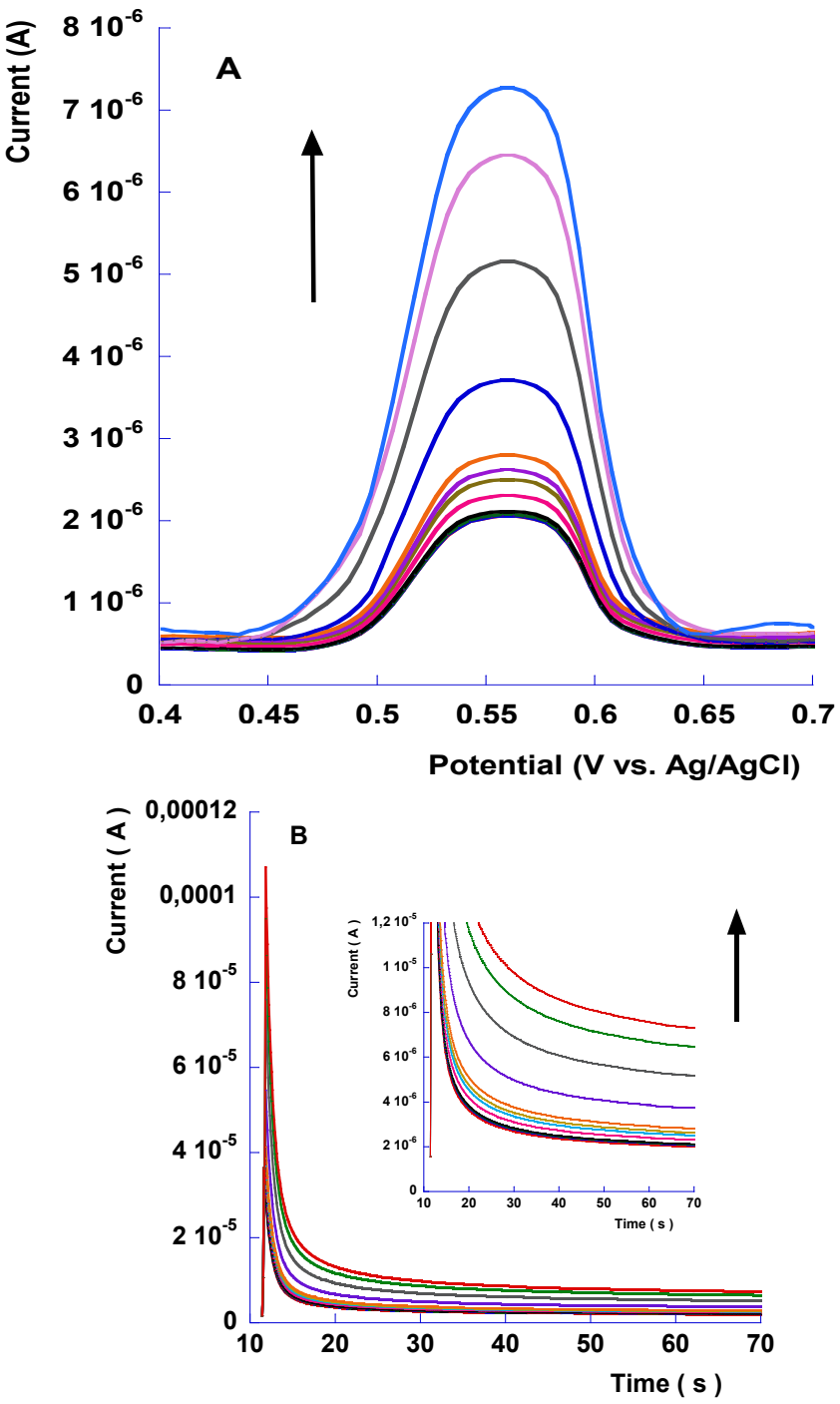

Fig. S4. Variation in the DPV current in the Ferrocene FC_4S/α-ApoE based immunosensor evidencing ApoE/α-ApoE recognition after incubation in ApoE solutions with gradually increasing concentrations (A) and variation in chronoamperometry current of Ferrocene FC_4S immunosensor after incubation in progressive ApoE concentrations (B).

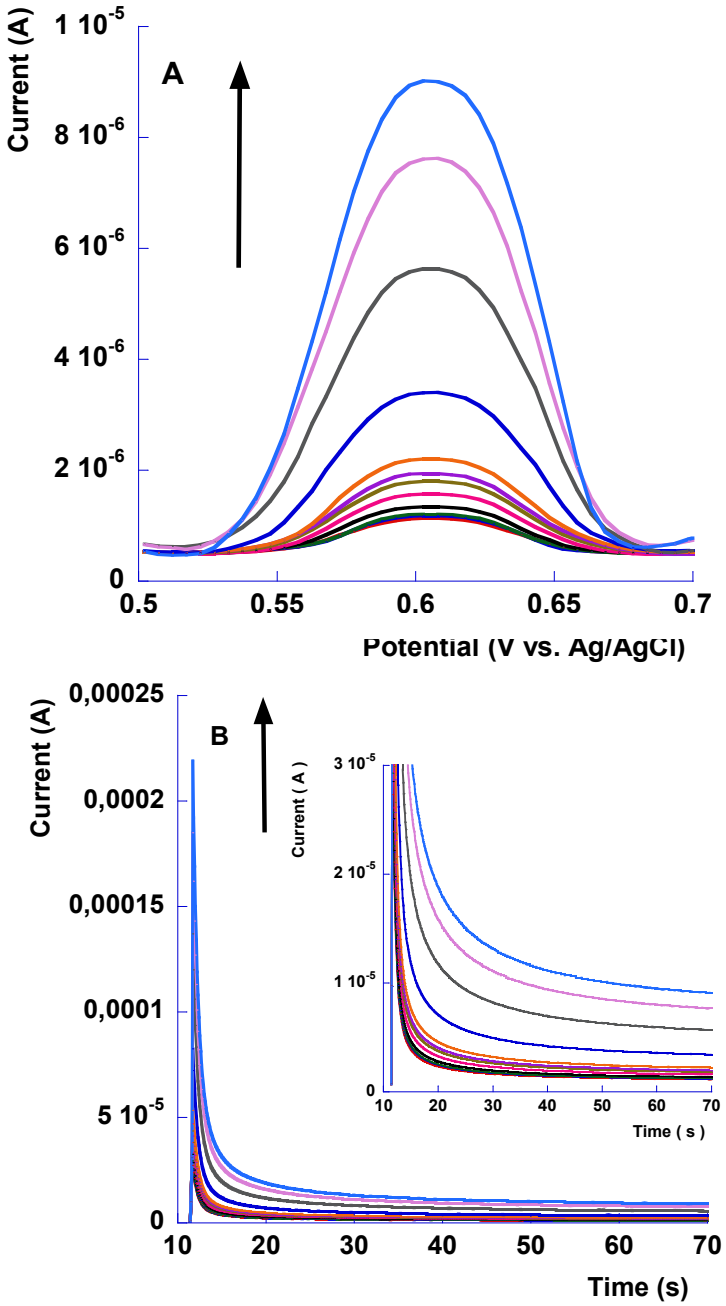

Fig. S5. Variation in the DPV current in the Ferrocene FC_8S/α-ApoE based immunosensor evidencing ApoE/α-ApoE recognition after incubation in ApoE solutions with gradually increasing concentrations (a) and variation in chronoamperometry current of Ferrocene FC_8S immunosensor after incubation in progressive ApoE concentrations (b).

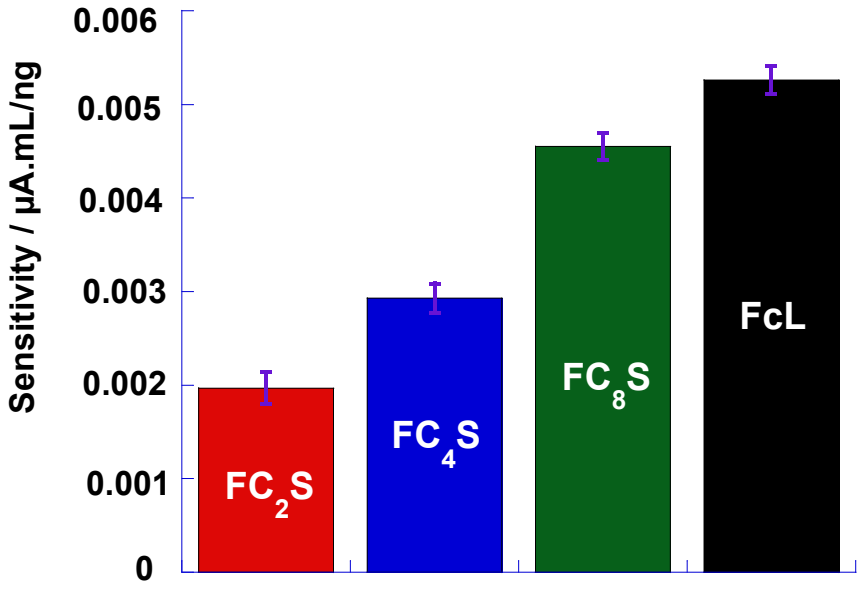

Fig. S6. Histogram depicting the sensitivity performances of the FC_2S, FC_4S, FC_8S and FcL-based ApoE biosensors obtained from chronoamperometry measurements

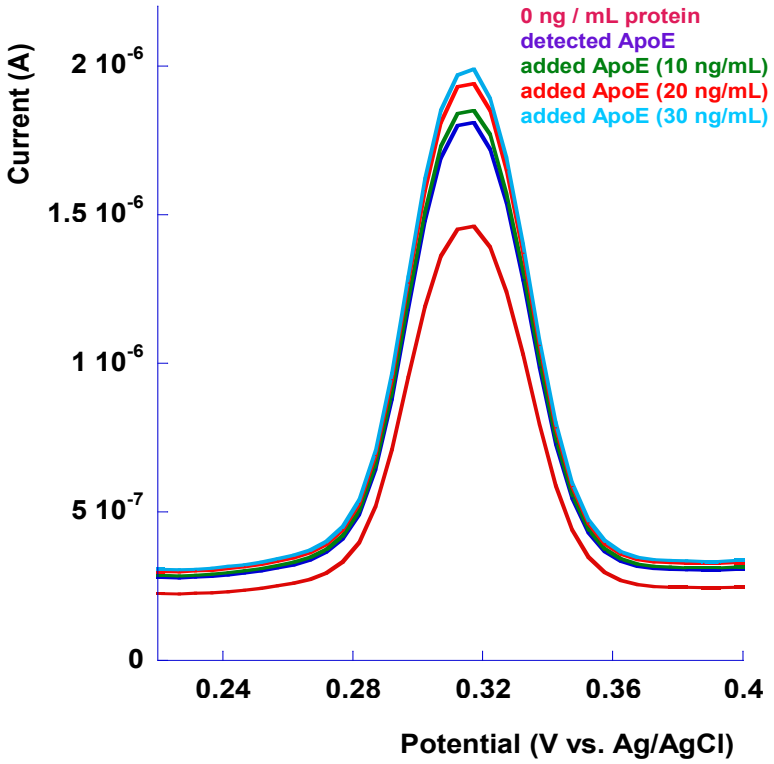

Fig. S7. Variation in the DPV current in the ApoE based immunosensor evidencing ApoE/α-ApoE recognition after incubation in diluted serum solution with gradually increasing ApoE concentrations.